Supplemental Information

Stabilizing $Li_{1.4}Al_{0.4}Ti_{1.6}(PO_4)_3$/Li Interface with In-situ constructed Multifunctional Interlayer for High Energy Density Batteries

*Can Huang [a], Shuo Huang [a],Aolai Wang [a], Ziying Liu [a], Dexuan Pei [a], Jianhe Hong [a], Shuen Hou [a], Levente Vitos [b], Hongyun Jin [a]**

[a] Engineering Research Center of Nano-Geo Materials of Ministry of Education, Faculty of Materials Science and Chemistry, China University of Geosciences, Wuhan 430074, China

[b] Department of Materials Science and Engineering, Royal Institute of Technology, Stockholm SE-100 44, Sweden

* Corresponding authors.

E-mail address: jinhongyun@cug.edu.cn (Hongyun Jin)

Experimental section:

1. Synthesis of the LATP pellets.

The LATP pellets were synthesized by the previously reported method.[1] The average thickness of the LATP pellets was 0.8 mm.

2. The modification of LATP.

The modification layer was realized by the drop-casting method. 0.25 g PVDF (Arkema, 5130), 0.10 g LiTFSI (Macklin, 99.9%), Mg_3N_2 (Aladdin, 99.5% metals basis) were mixed in 7 mL N, N-Dimethylformamide (DMF) solution (Aladdin, > 99.9% (GC)). The mixture was magnetically stirred for 10 h. Afterward, the precursor solution was dropped on the surface of LATP pellets. The modified pellets were then dried under 65 ℃ on hotplate for 1 h to evaporate the solvent. Since Mg_3N_2 is sensitive to moisture, all these operations were carried in an argon-filled glovebox (H_2O, O_2 < 0.01 ppm).

3. The preparation of cathode.

The $LiFePO_4$ cathode was prepared by mixing $LiFePO_4$, carbon black, and PVDF in NMP at a mass ratio of 6: 2: 2 and then coated on an Al foil. After drying at 70 ℃ in a vacuum oven, the foil was cut into pellets with a diameter of 10 mm. The pellet was further dried at 70 ℃ in a vacuum oven for 12 h. The areal loading of active materials is about 0.8 mg cm^{-2}. The high loading cathode was prepared with the mass ratio of $LiFePO_4$, carbon black, and PVDF at 8: 1: 1. The areal loading of active materials for high loading cathode is about 3.7 mg cm^{-2}.

4. Material and electrochemical characterization.

The structure of LATP were characterized by powder X-ray diffraction (XRD) pattern using a D8-FOCUS X-ray diffractometer with $CuK_{\alpha 1}$ radiation. The morphology and element analysis were acquired by a SU8010 field scanning electron microscope (SEM) and energy dispersive X-ray spectroscopy (EDS). To get the information about the element on the surface of LATP, X-ray photoelectron spectroscopy (XPS) was carried out by Thermo Scientific K-Alpha+ using Al Kα X-rays source (1486.6 eV).

CR2032 coin cells were assembled in an argon-filled glovebox (H_2O, O_2< 0.01 ppm) for electrochemical measurement. The sandwich structure that with the order of foamed nickel, Li metal chip, LATP, LFP, stainless steel sheet was adopted. 5 μL of liquid electrolyte (1 M $LiPF_6$ in EC: DMC = 1: 1) was added to the interface of LATP and cathode. Likewise, the symmetric cells were assembled.

All electrochemical impendence spectrum (EIS) was carried by Zennium X electrochemical workstation in the frequency range from 1 MHz to 1 Hz with a 40-mV amplitude. The SSLBs and the symmetric cells were conducted on a Wuhan Land battery tester. The tests for symmetric cells are conducted by charging for 0.5 h and then discharge for 0.5 h. CHI760E was carried out to measure cyclic voltammetry (CV) from 2.7 V to 4.1 V with a scan rate of 1 mV s^{-1}. All of these electrochemical measurements are carried at the temperature of 60 ℃.

5. Density Functional Theory (DFT) calculations.

All the self-consistent calculations were conducted based on the Vienna Ab-inito Simulation Package (VASP).[2, 3] The electron-ion interactions were described by the

full-potential projector-augmented wave (PAW) method, and the exchange-correlation interactions were described by the Perdew-Burke-Enzerhof (PBE) functional with the generalized gradient approximation (GGA).[4, 5] The vdW-D3 method developed by Grimme was employed to describe the van der Waals interaction.[6] The plane-wave energy cutoff was set as 450 eV. The convergence threshold was set as 1.0×10^{-6} eV in energy and 0.02 eV/Å in force. Slab models of Li (110), Li (001), Mg (002), Mg (100) and Mg (101) were built with three or four layers. A vacuum layer of 15 Å was adopted to avoid the periodic interactions. All atoms with adsorbates in the slab except the bottom one or two layers were allowed to relax. The Brillouin zone was modeled by gamma centered Monkhorst-Pack scheme, in which a 0.04/Å grid was adopted for all slab models.

The surface energy was calculated as follow:

$$\gamma = \frac{1}{2A}\left(E_{cleaved} - E_{bulk}\right) + \frac{1}{A}\left(E_{relax} - E_{cleaved}\right)$$

where the first part of right of formula raised due to bond breaking between atoms to create two new surfaces on either side of the vacuum slab, and the second part indicated the energy change due to atomic relaxation into stable positions in the vicinity of one of the formed surfaces.

For adsorption energy calculations, a Li atom was placed at 3 Å away from the surface, and the adsorption energy of a Li atom adsorbed onto each substrate was calculated as follow:

$$E_{ads} = E_{substrate+Li} - E_{substrate} - E_{Li}$$

where $E_{substrate+Li}$ is the total energy of a Li atom bound to the surface, $E_{substrate}$ is the

energy of the substrate, and E_{Li} is the energy per Li atom in bulk.

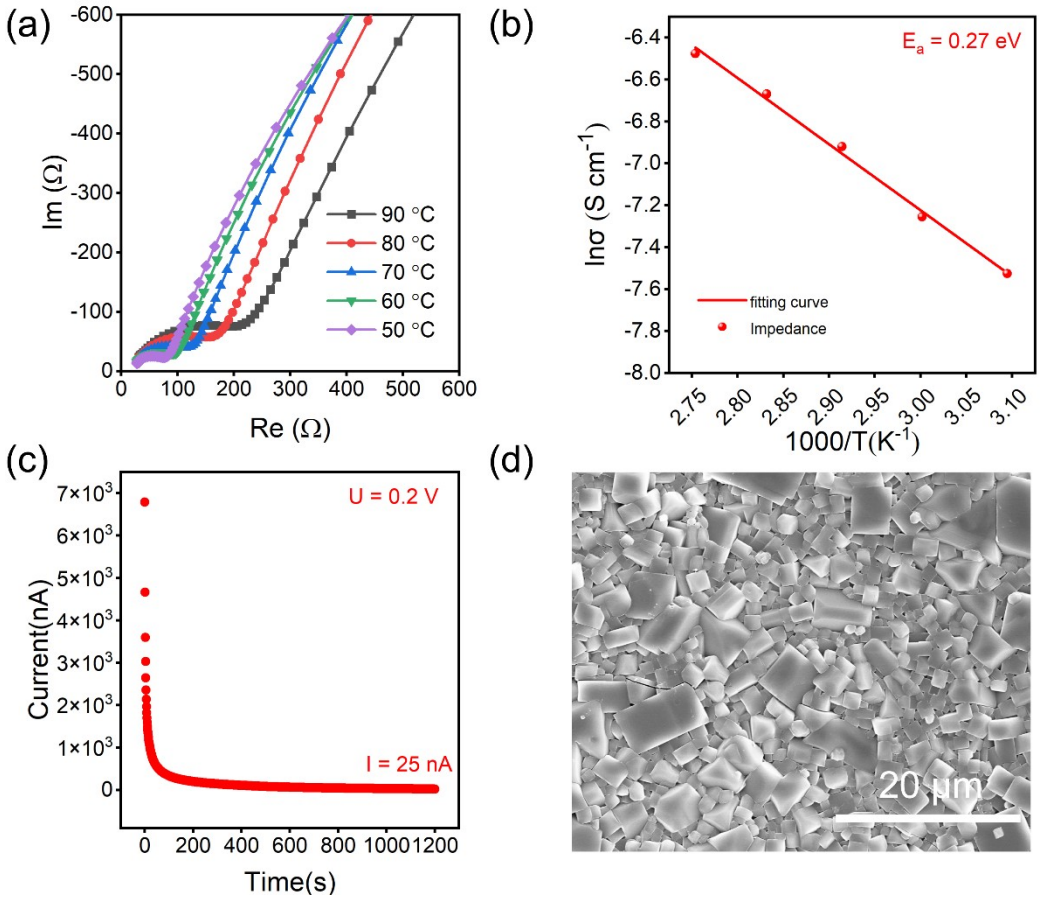

Fig. S1 (a) Nyquist plot at different temperature, (b) Arrhenius plot of ionic conductivity, (c) the evolution of current with polarization time under a polarization voltage of 0.2 V, and (d) surface morphology of LATP.

Fig. S2 Digital photo of MLATP pellet.

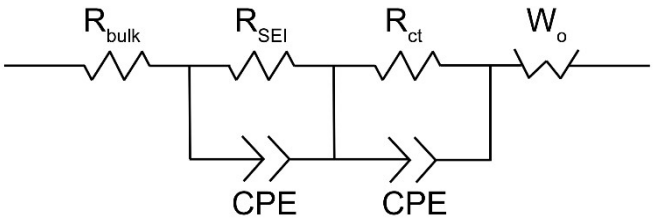

Fig. S3 The fitting equivalent circuit model.

Table S1 The fitting results of the symmetric cells.

		R_{bulk}	R_{SEI}	R_{ct}
Li/LATP/Li	before cycling	20.04	32.29	903.6
	after 48 cycles	230.80	1991.0	20513
Li/MLATP/Li	before cycling	15.99	169.1	1127
	after 100 cycles	67.60	312.0	186.2
	after 200 cycles	54.67	488.9	291.2
	after 400 cycles	79.56	666.4	571.4

Table S2 Comparison of electrochemical performance for the MLATP with recent works based on NASICON-type electrolytes.

	electrolyte	current density/ mA cm^{-2}	cycle time/ h	rate	cycle number	cathode loading/ mg cm^{-2}	Ref.
1	LATP	0.05	300	1	307	0.8	[1]
2	LAGP	0.1	100	0.5	100	1.5	[7]
3	LAGP	0.05	800	0.5	265	1.2	[8]
4	LATP	0.1	400	0.1	170	/	[9]
5	LAGP	0.2	800	0.2 (NCM811)	200	2	[10]
6	LATP	0.1	300	0.4	220	2.5	[11]
7	LAGP	0.1	150	1	100	/	[12]
8	LATP	0.2	1300	0.5	500	1.1	[13]
9	LAGP	0.15	800	0.5	100	1.2	[14]
10	LAGP	0.1	1000	0.1	40	2	[15]
11	LATP	0.2	1000	2	385	0.8	This work
				0.5	231	3.7	

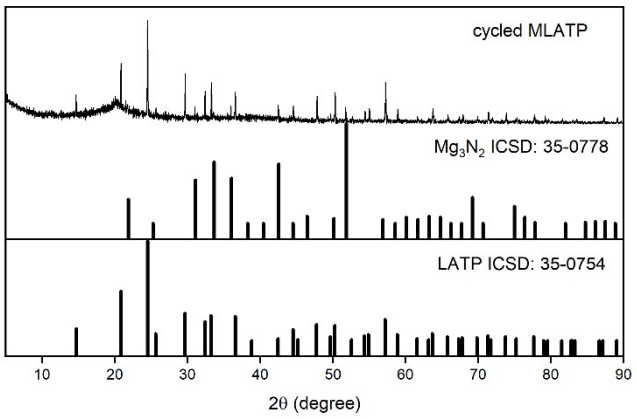

Fig. S4 XRD pattern of MLATP disassembled from the Li/MLATP/Li cell after 400 cycles at a current density of 0.20 mA cm^{-1}.

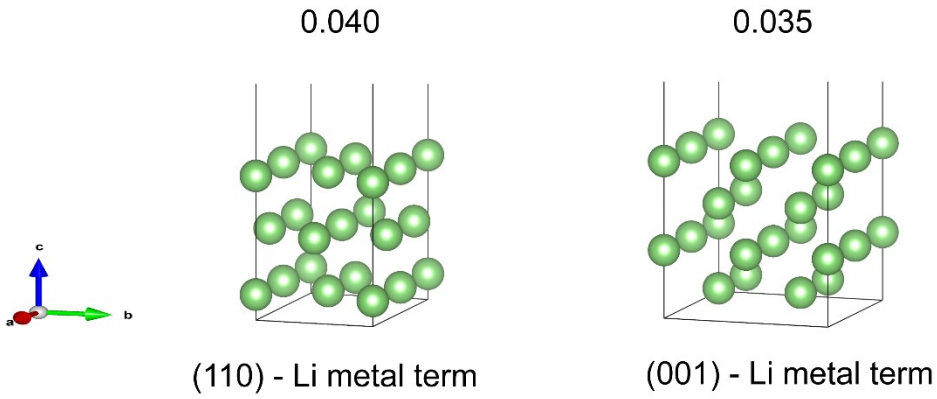

Fig. S5 Surface energy (eV $Å^{-2}$) of Li metal surfaces.

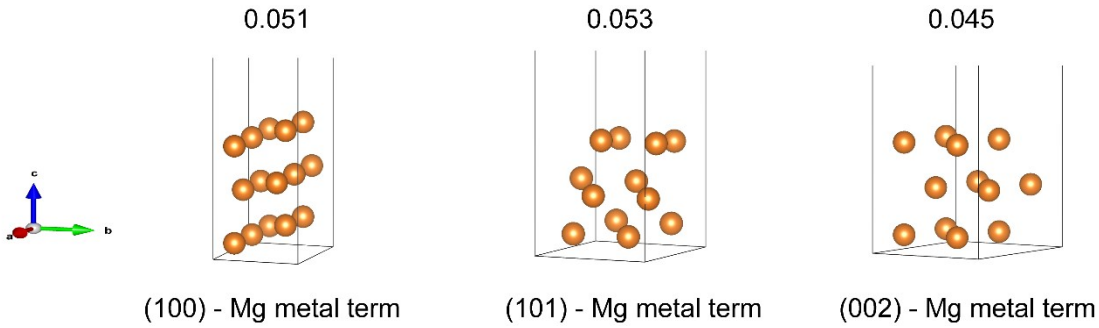

Fig. S6 Surface energy (eV $Å^{-2}$) of Mg metal surfaces.

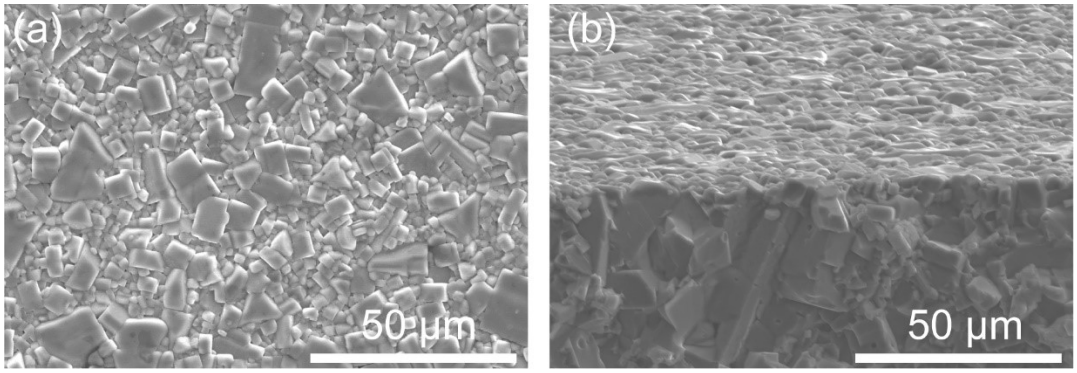

Fig. S7 (a) surface and (b) cross-section SEM images of LATP pellet disassembled from the Li/MLATP/Li symmetric cell after 400 cycles.

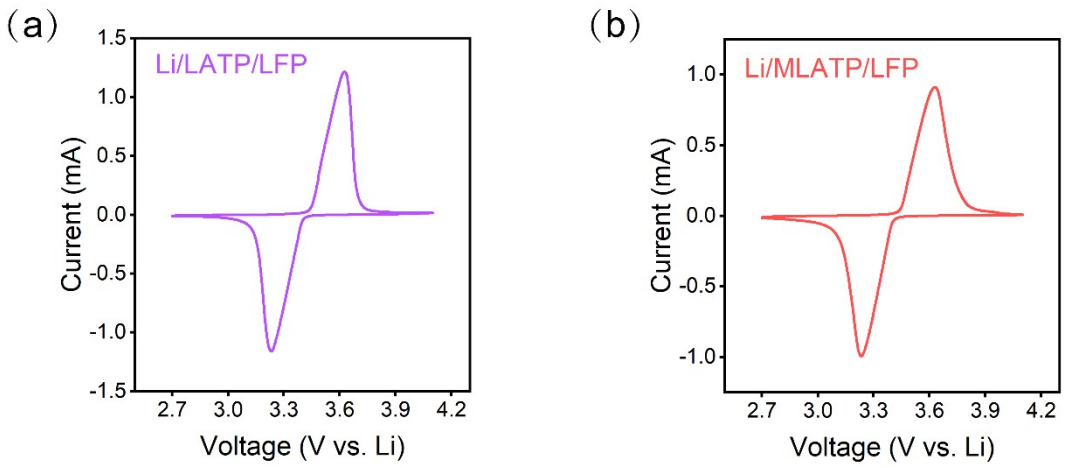

Fig. S8 CV curves of the (a) Li/LATP/LFP and (b) Li/MLATP/LFP cells

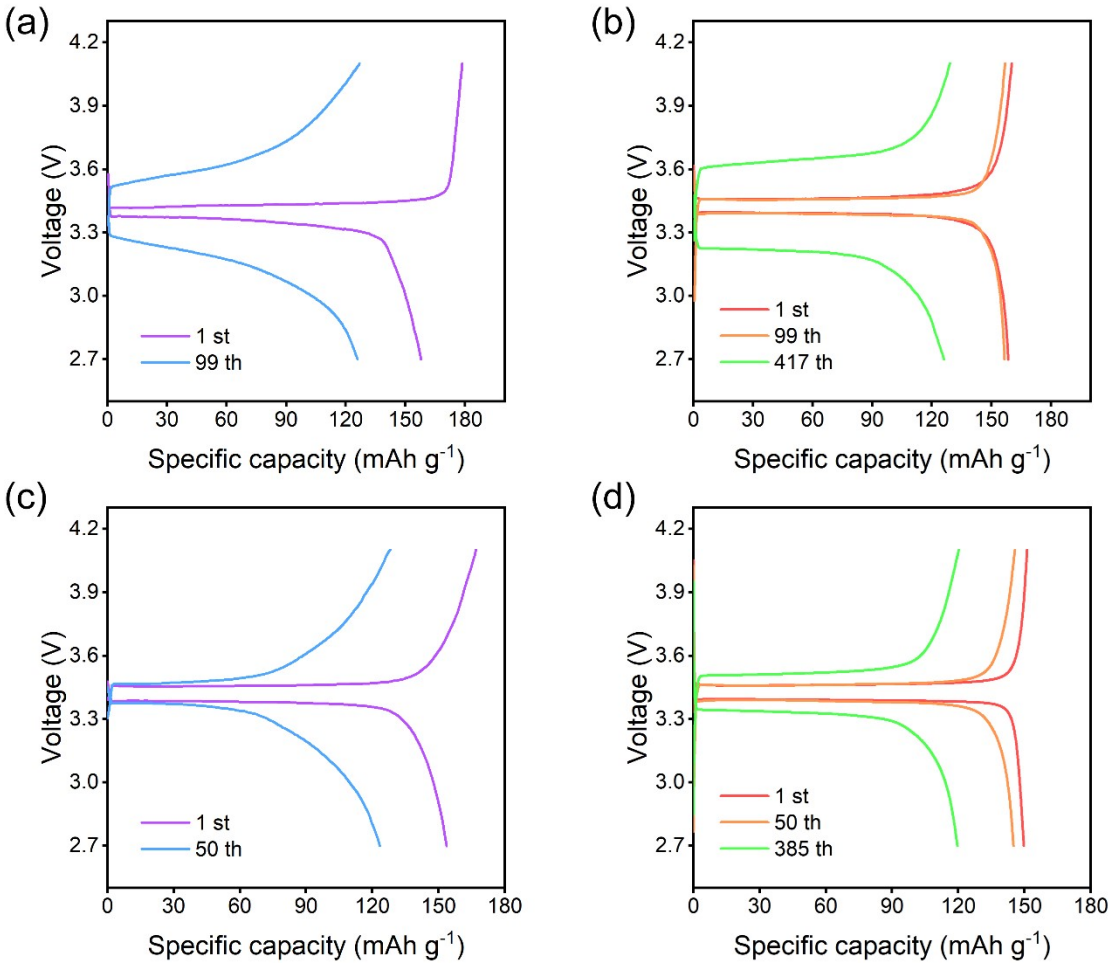

Fig. S9 The chare-discharge profiles of the (a) Li/LATP/LFP and (b) Li/MLATP/LFP cells at 1 C. The chare-discharge profiles of the (c) Li/LATP/LFP and (d) Li/MLATP/LFP cells at 2 C.

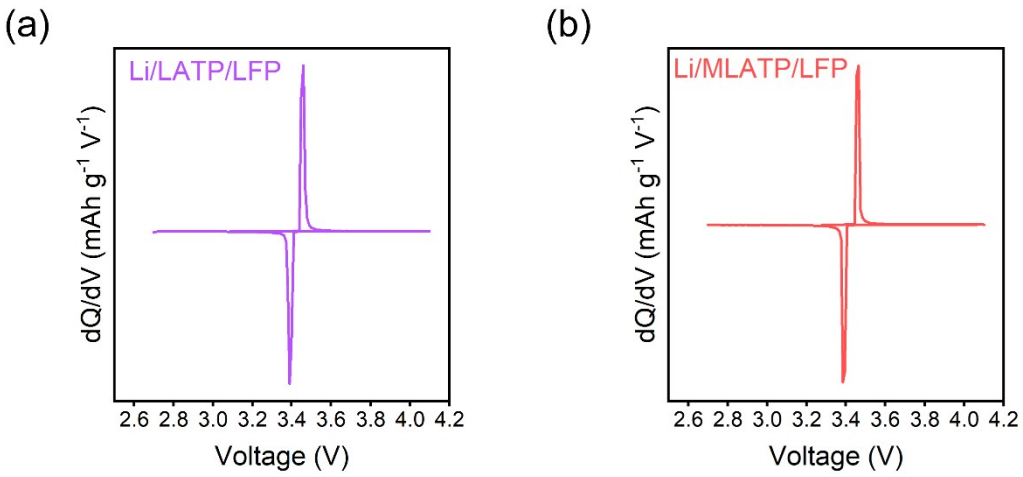

Fig. S10 The differential capacity curves of the (a) Li/LATP/LFP and (b) Li/MLATP/LFP cells for the first cycle.

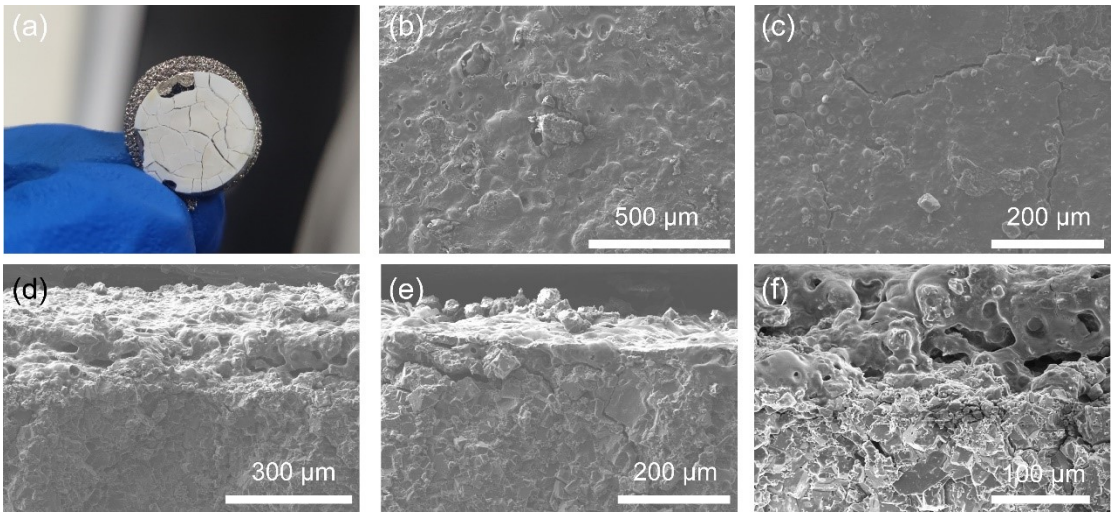

Fig. S11 (a) Digital photo, (b-c) surface SEM images, and (d-f) cross-section SEM images of LATP pellet disassembled from the Li/LATP/LFP cell after cycling at 1 C.

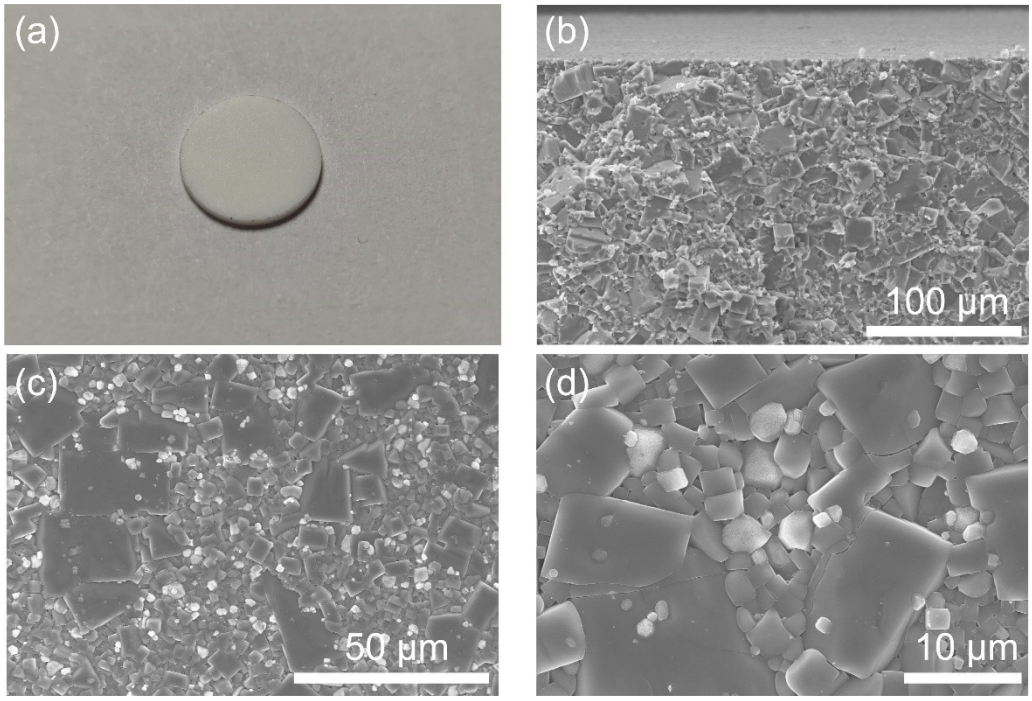

Fig. S12 (a) Digital photo and (b-d) SEM images of LATP pellet disassembled from the Li/MLATP/LFP cell after cycling at 1 C.

Table S3 The fitting results of the full cells.

		R_{bulk}	R_{SEI}	R_{ct}
Li/LATP/Li	before cycling	21.88	18.05	40.45
	after cycling	28.03	604.5	147.6
Li/MLATP/Li	before cycling	33.77	5.27	55.52
	after cycling	12.15	136.0	53.39

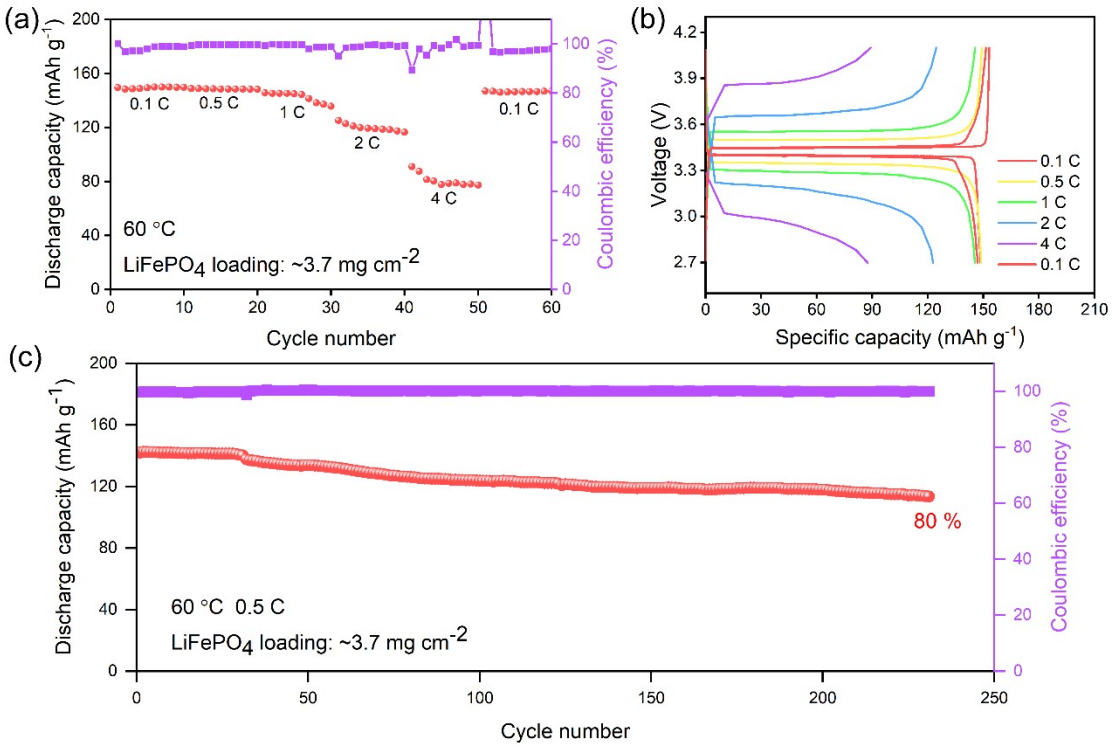

Fig. S13 (a) rate performance of the Li/MLATP/LFP full cell with a high mass loading cathode and (b) corresponding charge-discharge profiles, (c) the long-term cycle performance of the Li/MLATP/LFP full cell with a high mass loading cathode.

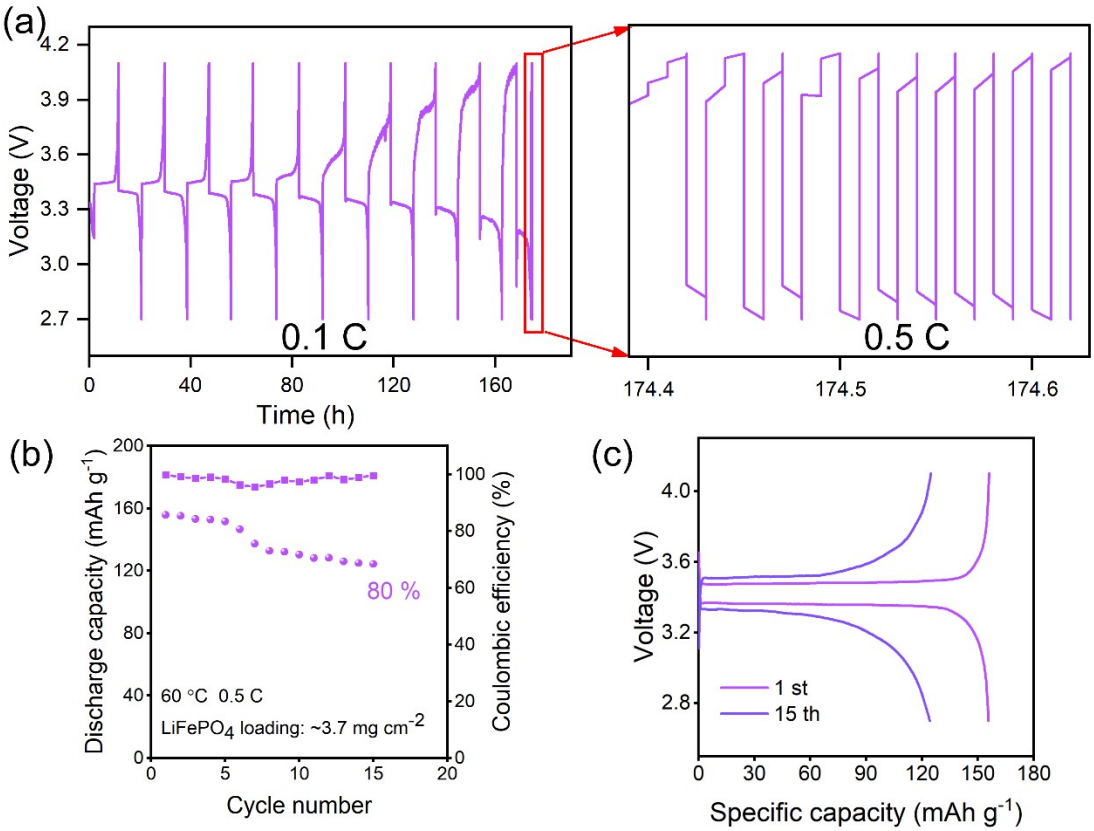

Fig. S14 (a) The charge-discharge profiles of the Li/LATP/LFP cell at 0.1 C and 0.5 C with the cathode mass loading of 3.7 mg cm^{-2}. (b) long-term cycle performance of the Li/LATP/LFP cell at 0.5 C with the cathode mass loading of 3.7 mg cm^{-2} and (c) the corresponding charge-discharge profiles.

Reference:

[1] C. Huang, Z. Li, S. Duan, S. Xie, S. Yuan, S. Hou, G. Cao, H. Jin, *J. Power Sources*, 2022, **536**, 231491.

[2] G. Kresse, J. Furthmüller, *Comp. Mater. Sci.*, 1996, **6**, 15-50.

[3] G. Kresse, J. Furthmüller, *Phys. Rev. B*, 1996, **54**, 11169-11186.

[4] P.E. Blöchl, *Phys. Rev. B*, 1994, **50**, 17953-17979.

[5] J. Perdew, K. Burke, M. Ernzerhof, *Phys. Rev. Lett.*,1996, **77**, 3865-3868.

[6] S. Grimme, J. Antony, S. Ehrlich, H. Krieg, *J. Chem. Phys.*, 2010, **32**, 154104.

[7] C. Li, Y. Chen, Z. Li, Y. Zhang, Z. Fang, J. Xu, Y. Sun, H. Bao, H. Cheng, *J. Power Sources*, 2021, **495**, 229765.

[8] S. Zhang, Z. Zeng, W. Zhai, G. Hou, L. Chen, L. Ci, *Adv. Mater. Interfaces*, 2021, **8**, 2100072.

[9] W. Cao, Y. Yang, J. Deng, Y. Li, C. Cui, T. Zhang, *Mater. Today Energy*, 2021, **22**, 100875.

[10] Z. Chen, H. Zhang, H. Xu, S. Dong, M. Jiang, Z. Li, G. Cui, *Chem. Eng. J.*, 2022, **433**, 1335899.

[11] M. Lei, S. Fan, Y. Yu, J. Hu, K. Chen, Y. Gu, C. Wu, Y. Zhang, C. Li, *Energy Storage Mater.*, 2022, **47**, 551-560.

[12] S. Lee, S. Jung, S. Yang, J.-H. Lee, H. Shin, J. Kim, S. Park, *Appl. Surf. Sci.*, 2022, **586**, 152790.

[13] L. Zhu, Y. Wang, Y. Wu, W. Feng, Z. Liu, W. Tang, X. Wang, Y. Xia, *Adv. Funct. Mater.*, 2022, **32**, 2201136.

[14] N. Ci, L. Zhang, J. Li, D. Li, J. Cheng, Q. Sun, Z. Xi, Z. Xu, G. Zhao, L. Ci, *Carbon*, 2022, **187**, 13-21.

[15] J. Yu, Q. Liu, X. Hu, S. Wang, J. Wu, B. Liang, C. Han, F. Kang, B. Li, *Energy Storage Mater.*, 2022, **46**, 68-75.